Available online at www.sciencedirect.com

ScienceDirect

Procedia Engineering 197 (2017) 214 – 223

Procedia Engineering

www.elsevier.com/locate/procedia

DYMAT 23rd Technical Meeting

Dynamic Fracture of Ductile Materials

Dynamic fracture behavior of high strength pipeline steel

Sarath Chandran[a], Patricia Verleysen[a*], Junhe Lian[b], Wenqi Liu[b], Steven Cooreman[c], Sebastian Münstermann[c]

[a]*DyMaLab, Department of Electrical Energy, Metals,Mechanical Construction and Systems, Ghent University, Technologiepark 903, Zwijnaarde, 9052 Gent, Belgium*
[b]*Steel Institute, RWTH Aachen University, Intzestraße 1, 52072 Aachen, Germany*
[c]*OCAS NV, ArcelorMittal Global R&D Ghent, Pres. J.F. Kennedylaan 3, 9060 Zelzate, Belgium*

Abstract

The occurrence of a crack propagating along a pipeline is a catastrophic event, which involves both economic losses and environmental damage. Therefore, the study of the fracture initiation and propagation properties of a pipeline is an essential part of its integrity assessment. Fracture prediction, however, is a challenging task, since it requires knowledge of the interaction between the dynamic forces driving crack growth, and the resistance forces opposing fracture propagation. Moreover, plenty of material properties should be taken into account. Aiming at a better understanding of the plastic hardening, damage and fracture properties of an API 5L X70 pipeline steel, and how these are affected by the strain rate, in present contribution, a comprehensive set of test results is presented. The program includes static and dynamic tensile tests on smooth and notched samples, and compression tests on cylindrical samples. Test result analysis is supported by finite element (FE) modelling. As such, the study aims at providing data needed for both fundamental material research and constitutive material modelling.

Peer-review under responsibility of the scientific committee of the International Conference on Dynamic Fracture of Ductile Materials

Keywords: Fracture propagation; plastic hardening; damage; strain rate; finite element; constitutive modelling

* Patricia Verleysen. Tel.: 0477537425; fax: 092643582.
E-mail address: Patricia.Verleysen@UGent.be

Peer-review under responsibility of the scientific committee of the International Conference on Dynamic Fracture of Ductile Materials
doi:10.1016/j.proeng.2017.08.098

1. Introduction

Steels utilized for the construction of oil and gas pipelines have to exhibit exceptional material properties to cope with severe working conditions. From a mechanical perspective, these conditions involve high internal pressures in the pipe, environmental temperatures far below the freezing point and high bending loads during offshore pipe laying. Legislative authorities obligate the suppliers and operators of the pipelines to meet high standards for environmental protection and safety by ensuring material and structural properties that conform to globally acceptable standards. One of these standards is the ISO 3183 of the International Organization for Standardization, defining steel grades including minimum values for strength and toughness, giving structural requirements like minimum wall thickness and setting the manufacturing requirements like the quality of the weld seams.

The occurrence of longitudinal cracks along gas pipelines has made it essential to have fracture propagation control to ensure pipeline integrity. Toughness tests such as Charpy tests and Battelle drop weight tests complemented by numerical simulation of ductile crack propagation and arrest are used to yield a conservative prediction of the fracture control strategy [1, 2]. The constitutive behavior of pipeline steels is often modelled taking into account quasi static conditions. However, Charpy and Battelle tests are dynamic events which require the knowledge of the strain rate sensitivity of the pipeline material. Additionally, very high strain rates can occur in the vicinity of a running crack in a high pressure gas pipeline. As such, the constitutive model has to account for strain rate sensitivity. The dependence of the fracture behavior on the strain rate of a commercial pipeline steel was extensively studied by S. de Luna et.al [3] wherein the material fracture toughness was found to increase slightly with strain rate. The analysis was also supported by micromechanical damage model. The important effect of the dynamic loading rates on the material resistance and on the tensile and initial toughness properties of steels was identified by C.S Wiesner et.al [4]. Increasing loading rates was observed to cause a shift from ductile fracture behavior at low rates to brittle behavior at high rates of loading and a method to predict this transition zone was also proposed. Moreover, a strain rate dependent cohesive zone finite element model has been developed to analyze the speed dependent fracture behavior of pipeline steels as observed in drop weight tear tests and to understand the dependence of the fracture toughness on crack speed which is critical for material selection and crack arrest design in high strength steel pipelines [5].The results suggested that strain rate effect in the bulk material could be largely responsible for the speed dependent dynamic fracture and model could be used to effectively predict the behavior. However, it has to be supplemented with sufficient experimental data in the dynamic ranges. Hence, it is imperative to have high strain rate tests for dynamic characterization of pipeline steels.

Conformance of the product with the applicable standards are ensured by performing a series of material and mechanical tests covering the entire range from small scale tensile tests to full scale burst tests under realistic conditions of use. Present study reports on an extensive experimental program that has been devised to characterize the plasticity, damage and fracture properties of an API 5L X70 pipeline steel. The program includes static and dynamic tensile tests on smooth and notched samples, and compression tests on cylindrical samples. Result analysis and interpretation is supported by finite element simulations of the tests.

2. Material and techniques

2.1. Test material

The material studied is an API 5L X70 pipeline steel provided by ArcelorMittal as hot rolled coil with a thickness of 14.8mm. The microstructure consists of a ferritic matrix with a low pearlitic content of 3%. All the samples are extracted in the rolling direction by mechanical machining.

2.2 Static testing

For the low strain rate experiments, an Instron material testing machine (Model 5569) is used. To ensure the same boundary conditions as in the dynamic tests, the samples are fixed between two slender loading bars in the same way as in the dynamic tests, see Fig. 1. Tests are performed at three different crosshead velocities, aiming at strain rates of 0.00025, 0.0025 and 0.025 s^{-1} in the central gauge or notch section of the samples. The lowest strain rate is selected in accordance with ISO 6892:1. Since the crosshead displacement systematically overestimates the actual sample deformation, three LVDTs attached to the loading bars are used to measure the sample elongation. The elongation measured by the LVDTs not only includes the deformation of the central section of the specimen but also of the transition zones and parts of loading bars. Therefore, additionally, digital image correlation (DIC) is used to obtain the local strain from a speckle pattern applied to the sample surface recorded during the deformation. The force is measured using a load cell with a capacity of 50 kN.

2.3 Dynamic testing

The high strain rate tests are carried out on split Hopkinson bar compression and tensile setups. Split Hopkinson bars are widely used to study the constitutive, damage and fracture behavior of materials at strain rates from 100 s^{-1} up to 10000 s^{-1}. Strains exceeding 100% can be achieved in tension, compression and shear. One of the main characteristics of Hopkinson experiments, in comparison with other high strain rate test techniques, is that a high strain rate deformation is imposed while the sample is in dynamic equilibrium. Indeed, if the sample is sufficiently small, wave propagation effects can be neglected in the sample. Additionally, the determination of the force on the specimen is done without the use of a load cell and the measurement of the specimen elongation is made without directly monitoring the specimen length.

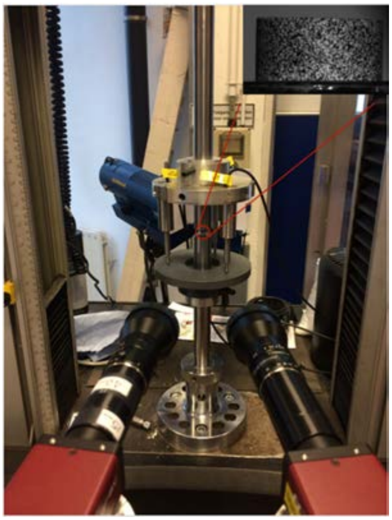

Fig. 1. Setup used for the static tests with detailed image of a compression sample with speckle pattern used for local DIC strain measurement.

Fig. 2. Split Hopkinson tensile bar setup of DyMaLab of Ghent University.

The concept of the split Hopkinson bar setup involves a test sample sandwiched between two long bars, an input and output bar. For tensile tests, most often, a tube-like impactor is put around the input bar and is accelerated towards an anvil at the outer end of the input bar. Thus a tensile wave, the so-called incident wave, is generated and propagates along the input bar towards the specimen. For compression tests, a cylindrical bar impactor is utilized instead of a tube impactor. The impactor is positioned in line with the input bar and accelerated towards the input bar resulting in an incident compressive wave. The strain rate in the sample can be adjusted by the velocity of the impactor.

The incident wave interacts with the specimen, generating a reflected wave and a transmitted wave. The incident, reflected and transmitted wave are measured, usually by means of strain gages, at well-chosen locations on the Hopkinson bars. From these waves, the total force and elongation history of the specimen can be determined based on the principle of one dimensional elastic wave propagation in slender bars [6]. For uniaxial tensile or compression tests, the strain in the sample is often calculated by dividing the elongation by the length of the gauge section. However, this gives rise to an overestimation of the strain, especially for dog bone shaped tensile samples [7]. Therefore, and also to monitor the highly non-homogeneous strain fields in the notched samples, also for the dynamic tests a local strain measurement is used based on high speed camera imaging and DIC.

A picture of the DyMaLab split Hopkinson tensile bar (SHTB) setup is presented in Fig. 2. The setup was designed for large deformation materials; its total length of 11m allows loading times up to 1.2milliseconds.

2.4 Finite element modelling

To come to an in-depth understanding of the experimental results, finite element models have been built of the test configurations using the commercial program Abaqus/standard. The samples are modelled using C3D8R solid elements with an average size of 0.1 mm in the critical notch or gauge section. With the selected mesh size, acceptable convergence and mesh sensitivity are obtained. To describe the materials constitutive response, J2-plasticity is adopted wherein the flow curve from the slowest static test is used for hardening. True stress and plastic strain data up to the point of necking are entered in a tabular format for the material model. Boundary conditions similar to those in the actual tests are implemented. The displacement is imposed on one end of the specimen.

3. Test program

In the test program a wide range of strain rates and stress states is considered to assess the strain rate sensitivity and damage properties of the material. For each sample geometry, both the quasi static and dynamic tests are performed at three different strain rates. Two tests are performed for each test condition.

For static tests, generally, standardized geometries are proposed, however, these geometries cannot be adopted for the high strain rate tests due to the limitations imposed by the test setup. Indeed, high strain rate tests need small specimens. Since, different specimen geometries for different strain rates are not desirable for reasons of comparability, the same specimen geometries are utilized for the dynamic and static tests. In this way, the influence of sample geometry effects is excluded. Moreover, the same technique is adopted for connecting the samples to the test setup thereby eliminating any disparity due to imposed boundary conditions. The sample geometries employed for testing of the X70 pipeline steel are discussed in the following sections.

3.2.1. Smooth and notched tensile specimens

The general shape of the tensile specimens is a cylindrical dog bone with a minimum diameter of 2.5mm. The smooth specimen used to characterise the strain rate dependent plastic hardening of the X70 steel, features a parallel gauge section with a length of 6mm and diameter of 2.5mm, see Fig. 3. The radius of the transition zone between the parallel gauge section and machined threads is 1.5mm. To assess the materials damage and fracture properties, three notched samples are used, see Fig. 4. The notches give rise to non-axial stresses and thus higher triaxialties. For the notched samples, the diameter of the shoulders next to the notch is 4.5mm and the minimum diameter beneath the deepest point of the notch is again 2.5mm. Notch radii of 0.5, 1 and 2.5mm are employed, see Figs. 4. To mount the specimens between the Hopkinson bars, all tensile specimens have a M8×1.25-6g thread.

Fig. 3. Smooth dog bone tensile specimen.

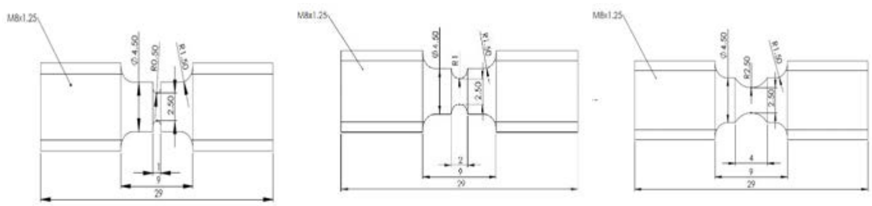

(a) (b) (c)

Fig. 4. Notched tensile specimen geometries with notch radii of (a) 0.50mm, (b) 1mm and (c) 2.50mm.

3.2 Compression Specimen Geometry

For the quasi static and dynamic compression tests, a cylindrical specimen with a diameter of 4mm and height of 4mm is used, see Fig. 5. The dimensions are the result of a compromise between the requirements imposed by the reduction of the influence of friction in the setup/sample interfaces and reaching sufficiently high strain rates in the Hopkinson tests [6, 8, and 9].

Fig. 5. Cylindrical compression specimen.

4. Results and analysis

4.1 Smooth dog bone tests

Fig. 6 shows representative engineering stress-strain curves obtained for the investigated steel grade at strain rates ranging from the quasi static to the dynamic regime. As mentioned, strain rates of 0.00025, 0.0025 and 0.025s^{-1} are imposed under static testing and 550, 900 and 1100s^{-1} under high strain rate conditions. The latter strain rate values are averaged values during plastic deformation.

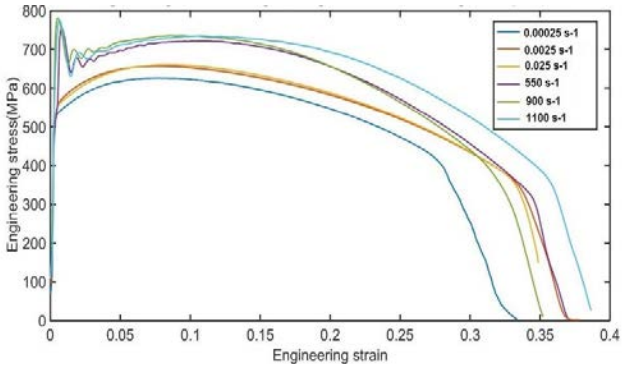

Fig. 6. Representative engineering stress-strain curves for the smooth tensile specimens.

From Fig. 6, it can be seen that both yield stress and tensile strength are found to increase with the strain rate. The most pronounced differences in strength levels are observed between the static and dynamic tests. The influence of the strain rate is less significant in the dynamic range compared to the quasi static regime. Relative deformation rates between static and dynamic tests might be a possible explanation however, transition from isothermal to adiabatic heating at higher strain rates causes a localised temperature increase and diminishes the rate effect on flow stress. It is interesting to note that the exceptional stress levels at high strain rates are reached without loss in material ductility in comparison with the quasi static tests. On the contrary, both the uniform elongation and the fracture strain are higher in the dynamic tests. This observation is confirmed by measurement of the local strain by DIC and the fracture surface.

4.2 Notched round bar tests

Figs. 7 present the quasi static and dynamic engineering stress-displacement curves for the three notched samples. The engineering stress is the average tensile stress in the notch, obtained by dividing the force by the initial area of the notch section. In line with the multiaxial stress states in the notches, the stress levels are significantly higher than these obtained for the smooth samples (Fig. 6) and increase with increasing notch sharpness.

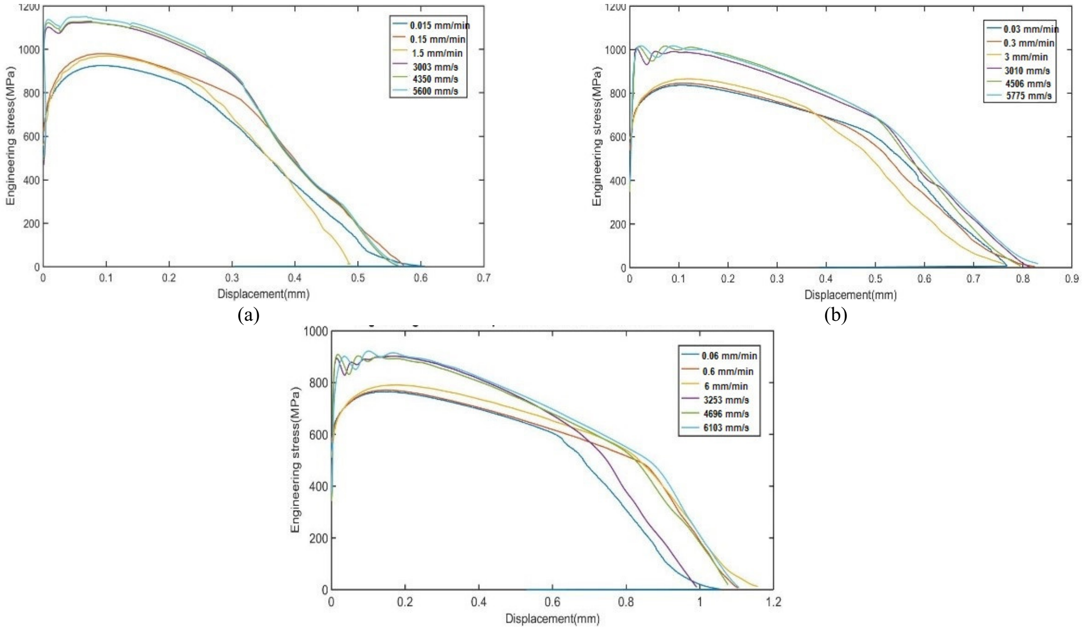

Fig. 7. Quasi static and dynamic engineering stress-displacement curves for samples with notch radii of 0.50mm (a), 1mm (b) and 2.5mm (c).

As is the case for the smooth tensile samples, for all notched samples the influence of the strain rate is considerable during the transition from static to dynamic deformation rates. However, when only the dynamic tests are considered, the strain rate sensitivity is very low, even negligible. Similar deformation levels are observed at both static and dynamic conditions for R1 and R0.50 notch, however, some loss in deformation capacity is exhibited by R2.50 notched samples at higher strain rates. From all the tests it is clear that the non-axial stresses in the notches have a detrimental effect on the material's ductility. Indeed, sharper notches give rise to higher triaxialities, which, as can be seen in Figs. 7, clearly results in drastic reduction of the deformation levels. These observations are confirmed by the values of the fracture strain which will be discussed in section 4.5.

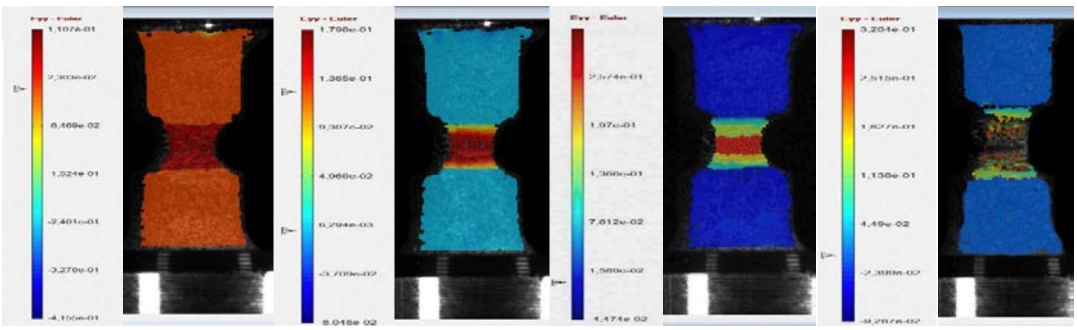

Fig. 8 Digital image correlation for a notched specimen with radius 1.0 mm at various stages of deformation

Fig 8 shows the images of the digital image correlation obtained for a notched specimen with radius 1.0 mm at various extents of deformation (in fig 8; deformation in sequence, u (in mm) =0.08, 0.17, 0.32 and 0.74 respectively) to the point of failure.

4.3 Effect of stress state

As mentioned, the notched tensile geometries are designed to cover wide and discrete ranges of stress states, reflected in significantly different stress triaxialities in accordance with the Bridgman Equation [10]. With the sample dimension given in Fig. 3, initial triaxialities of 0.33, 0.56, 0.82 and 1.14 are obtained for respectively the smooth, R2.50, R1.0 and R0.50 tensile specimen geometries. However, the triaxiality is not homogeneously distributed in the sample gauge or notch section and evolves during deformation. Finite element simulations of the different geometries, see Figs. 9, are performed to identify the distribution and evolution of the triaxiality.

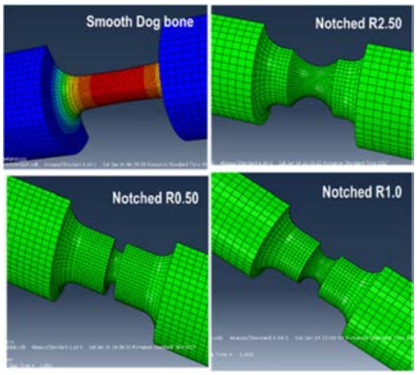

Fig. 9. Finite element models of the X70 pipeline tensile specimens.

In Fig. 10 plots are presented of stress triaxiality in the centre of the four tensile samples as a function of the Mises plastic equivalent strain (PEEQ). Starting from the values given by Bridgman's equation, the triaxialities rapidly increase during deformation, reach a maximum and, after a slight drop, remain relatively stable.

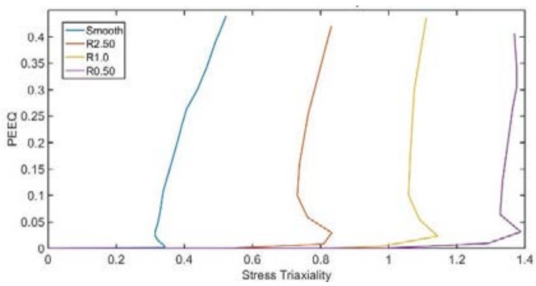

Fig. 10. Evolution of stress triaxiality is a function of the Mises plastic equivalent strain for all –smooth and notched- tensile samples.

4.4 Effect of strain rate

To further demonstrate the strain rate sensitivity of the X70 steel, Fig. 11 presents the tensile strength as a function of the logarithm of the strain rate. Both static and dynamic tests are considered on smooth and notched tensile samples. The strain rate clearly has a positive influence on the maximum tensile stress. Furthermore, the strain rate sensitivity seems to increase with the sharpness of the notch.

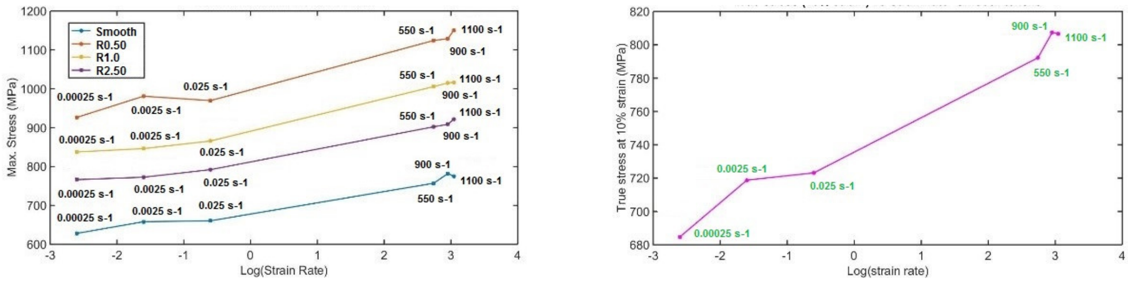

(a) (b)

Fig. 11. (a) Maximum stress versus strain rate for tensile specimens. (b) True stress (10% strain) versus strain rate for smooth tensile specimen.

Fig. 11 (b) provides the true stress for the smooth dog bone tensile specimens at 10% of strain with respect to strain rate. True stress is determined based on the equation 1.

$$\text{True stress} = \text{Engineering stress} * (1 + \text{Engineering strain}) \qquad (1)$$

Strain rates spanning both static and dynamic ranges are considered. It is clear that the value of the true stress at a specific percentage strain (10% in this case) increases with rise in strain rates. Though, as is also the case for the tensile strength, the true stress slightly drops for the highest strain rates.

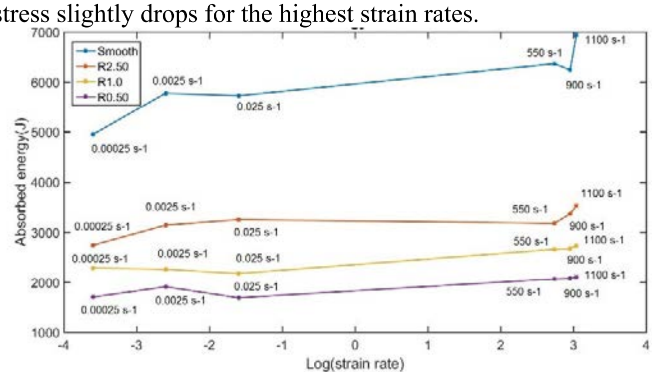

Fig. 12. Absorbed energy by smooth and notched tensile specimens as a function of strain rate.

The strain rate also has a clear impact on the energy absorbed by the material, as can be seen in Fig. 12 where the absorbed energy is presented as a function of the strain rate for the smooth and notched samples. The absorbed energy is calculated as the area under the experimental force-displacement curves. Varying dependencies of the absorbed energy on the strain rate are observed in the static regime. However, in the dynamic regime, the absorbed energy consistently increases with strain rate. Comparison of the absolute values of the absorbed energy between the different samples is not relevant because for each sample, and even strain rate condition, different material volumes are involved in the energy dissipation process. However, Fig. 12 shows that the effect of the strain rate in the dynamic regime is most pronounced for the smooth samples.

4.5 Fracture strain

The detrimental effect of the multiaxial stress states imposed by the notched specimen geometries on the displacements, as displayed in Figs. 7, does not necessarily reflect the material response. Indeed, the sharper the notch, the more the deformation is concentrated around the notch. Therefore, to assess the influence of the stress state on the ductility, post mortem, the fracture surfaces have been observed. For the smooth tensile samples and some of the notched samples, a cup and cone fracture behaviour is observed. Fully ductile fracture characteristic was observed from the fracture surface and the material did not exhibit any sign of anisotropy. Fig. 13 exhibits a fractured smooth tensile specimen tested at 900 s^{-1}.

Fig. 13. Smooth dog bone tensile fractured specimen.

From the fracture surfaces, the fracture strain can be calculated by:

$$\varepsilon_f = \ln\left(\frac{A_0}{A_f}\right) = 2\ln\left(\frac{d_0}{d_f}\right) \qquad (2)$$

With A_0 (d_0) and A_f (d_f) respectively the cross sectional area (diameter) of the initial and fractured section. The thus obtained fracture strain is an average value of the fracture strain. The reduced diameters are measured at eight different points along the circumference of the fracture surface and averaged to obtain d_f used to calculate the fracture strain.

The fracture strain is one of the most interesting fracture properties since it quantifies the materials deformation capacity unambiguously. Table 1 displays the average fracture strain calculated from the tensile experiments. These fracture strain values show that the stress state, indeed, has a negative influence on the material response in terms of deformation capacity. Moreover, also the higher ductility in dynamic conditions is confirmed.

Table 1 Average fracture strains observed in the tensile experiments

Specimen geometry	Dynamic	Static
Smooth dog bone tensile	1.15935	1.06824
Notched round bar with radius 2.50	0.91256	0.87829
Notched round bar with radius 1.0	0.48667	0.46464
Notched round bar with radius 0.50	0.20875	0.18853

4.6 Compression Testing

The cylindrical specimens are tested on a split Hopkinson compression setup aiming at strain rates of 400, 700 and 1000s^{-1}. Sufficient lubrication (Grease or Teflon low friction coatings) is applied at the interface of the bars with specimen surfaces to combat the effect of friction during compression testing. Engineering stress-strain curves are presented in Fig. 14(a). Only a marginal increase of the stress levels with the strain rate is observed. Since no sample failed during testing, the highest value of the strain cannot be interpreted as the failure strain, it gives the deformation that can be achieved by the one single wave. Fig. 14(b) illustrates the true stress-effective plastic strain response of the compression samples at high strain rates.

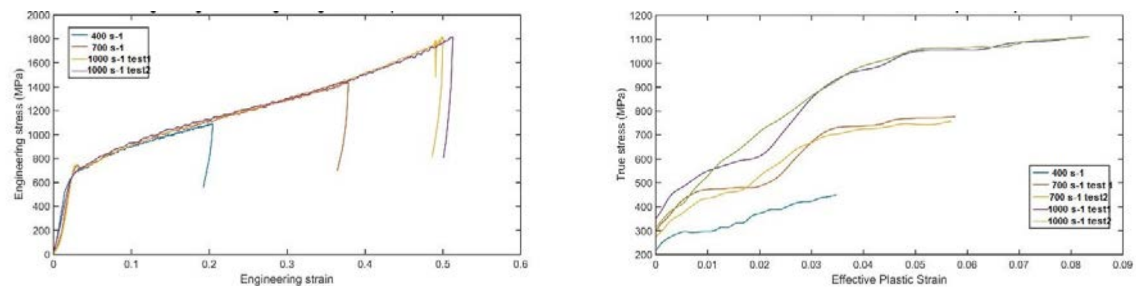

(a) (b)

Fig. 14. (a) Engineering stress versus engineering strain (b) True stress versus effective plastic strain for compression samples.

Here as well, true stress is calculated with the help of equation 1 and equation 3 is utilised to evaluate the effective plastic strain from the test

$$\text{Effective plastic strain} = \text{True strain} - (\text{TrueStress}/\text{E}) \quad (3)$$

Where E is the Young's modulus of the material ; E=207 GPa (ASTM A370) and true strain is given by equation 4

$$\text{True strain} = \ln(1 + \text{Engineering strain}) \quad (4)$$

From the experimental series, flow stress and fracture strain were observed to increase with strain rate because at higher rates, strain rate in the neck region becomes significantly larger than the initially imposed strain rate. The increased strain hardening ability will enhance the local deformation in the neck region. This deformation localisation together with increase in local strain rate lead to higher local flow stress and higher elongation. Moreover, strengthening effect induced by higher strain rate delays the onset of thermal softening thereby aiding absorption capacity.

5. Conclusion

Results are presented of an extensive, experimental study into the strain rate and stress state dependent material behaviour of an X70 pipeline steel. Static and dynamic tensile tests are performed on smooth and notched samples, compression tests on cylindrical samples. From the test results and analysis, the following conclusions can be drawn:

- The material combines a high strength with a relatively high ductility. The strength increases with the strain rate along with a relative increase in deformation capacity. However, the energy dissipated by the material is still higher at dynamic strain rates compared to the quasi static rates. The material, consequently, possesses a high energy absorption potential, even in dynamic conditions.
- The influence of the strain rate on the material behaviour is especially important when comparing static with the dynamic testing conditions.
- For all samples, including the samples with sharp notches, at all strain rates, a ductile fracture is observed.

Acknowledgement

The research leading to these results has received funding from the Research Fund for Coal and Steel (RFCS) of the European Commission (Toolkit project).

References

[1] R.H.Talemi, M. Steinhoff, S. Cooreman, F. Van den Abeele, P. Verleysen (2016) Effects of high strain rates on the ductile slant fracture behaviour of pipeline steel: Experiments and Modelling, Proc 11th Int Pipeline Conf (IPC)

[2] F. Van den Abeele, J. Peirs, P. Verleysen, F. Oikonomides, J.V. Wittenberghe (2012) Dynamic behaviour of high strength pipeline steel, Proc 9th Int Pipeline Conf (IPC)

[3] S de Luna, J Fernandez Saez, J.L.P Castellanos, C. Navarro (2000), An analysis of the static and dynamic behaviour of a pipeline steel, International Journal of Pressure Vessels and Piping, Vol.77, Issue 11, 1 September 2000, pp 691-696.

[4] C.S Wiesner, H.Macgillivray (1999), Loading rate effects on the tensile properties and fracture toughness of steel, TAGSI seminar, Fracture, Plastic flow and structural integrity, TWI, Cambridge, UK, 29 April 1999.

[5] P.S Yu, C.Q. Ru (2014), A strain rate dependent finite element model of drop weight tear tests for pipeline steels, 10th International Pipeline Conference, Volume 3: Materials and Joining ; Risk and Reliability, ISBN: 978-0-7918-4612-4, IPC2014-33047, pp. V003T07A002.

[6] H. Kolsky (1949) An investigation of the mechanical properties of materials at very high rates of loading. Proc Phys Soc London B 62 676-700.

[7] P. Verleysen, J. Degrieck (2004) Experimental investigation of the deformation of Hopkinson bar specimens. Int J Imp Eng 30 239-253

[8] E.D.H. Davies, S.C. Hunter (1963) The dynamic compression of solids by the method of the split Hopkinson pressure bar. J Mech Phys Solids 11 155-179.

[9] A.S. Khan, J.E. Balzer, J.M .Wilgeroth, W.G. Proud (2014), Aspect ratio compression effects on metals and polymers, 18th APS SCCM and 24th AIRAPT, Journal of Physics: Conference series 500 : 182019

[10] P.W. Bridgman (1952) Studies in large plastic flow and fracture. Cambridge, MA: Harvard University Press.